PCCP

RSC Publishing

PAPER

View Article Online
View Journal | View Issue

First principles study of the permeability of graphene to hydrogen atoms

Cite this: *Phys. Chem. Chem. Phys.*, 2013, **15**, 16132

Meng Miao,[a] Marco Buongiorno Nardelli,[b] Qi Wang[a] and Yingchun Liu*[a]

Received 3rd June 2013,
Accepted 30th July 2013

DOI: 10.1039/c3cp52318g

www.rsc.org/pccp

Using calculations from first principles and harmonic transition state theory, we investigated the permeability of a single graphene sheet to protons and hydrogen atoms. Our results show that while protons can readily pass through a graphene sheet with a low tunneling barrier, for hydrogen atoms the barriers are substantially higher. At the same time, the presence of defects in the membrane can significantly reduce the penetration barrier in a region that extends beyond the defect site itself.

I. Introduction

Graphene, a truly two dimensional carbon material, has attracted extensive research for its unique electronic, thermal and mechanical properties[1] and potentially revolutionary applications of graphene are sought in various technological fields. The study of graphene hydrogenation and understanding of the mechanism of interaction between graphene and hydrogen are of importance for a broad class of applications. A controlled adsorption of hydrogen atoms over the whole graphene surface leads to formation of a two-dimensional hydrocarbon, graphane,[2] a material with a direct band gap of $\sim$3.5 eV, as opposed to the gapless band structure of graphene. Opening a band gap through controlled hydrogenation could be an essential element for the development of a graphene field-effect transistor.[3] Partially hydrogenated graphene can act as a precursor for the formation of conducting and semiconducting nanorods and for graphene nanoribbons (GNR), with varying widths and orientation of the edges, they can be magnetic, semiconducting or metallic.[4] In addition, the interaction of hydrogen with graphene/graphite is important in hydrogen storage applications[5] and for thermalization and cooling in nuclear fusion devices,[6,7] as the hydrogen plasma erodes the divertor and then undesirable hydrocarbon impurities are generated.

Adsorption and diffusion of H on graphene have been studied by numerous authors: Herero *et al.*[8] demonstrated that quantum effects enhance the hydrogen diffusivity in the graphene sheet by a factor of 20 at room temperature; Miura *et al.*[9] showed that the reconstructions of carbon atoms play an important role in H adsorption and determine the effective pathway of diffusion and bonding on the graphene surface. H diffusion routes[10] into a graphene sheet and the kinetic properties[11] of H in graphene have also been investigated using first principles techniques. Given its peculiar two-dimensional character, graphene can be considered as an ideal membrane. Experimental efforts[12] and theoretical investigations[13] have shown that perfect graphene sheets are impermeable to standard gases, including small atoms like He. Similarly, the large energy barriers prohibit Li diffusion through the sidewalls of pristine nanotubes.[14] It can even offer a unique separation barrier between two distinct phases.[12] However, the penetration barriers decrease exponentially with the size of the defects for He.[13] In other words, porous graphene allows smaller molecules to pass through but excludes larger molecules, and can be used for gas separation.[15–17] Moreover, nanoporous functionalized graphene with nitrogen atoms in a nanosized ring pore has been shown to separate the isotope ^{3}He from ^{4}He by quantum tunneling through the pore.[18] In this work we focus on the penetration mechanism of hydrogen (which, with its Bohr radius of 0.5 Å, is much smaller than the distance between meta carbon atoms in the hexagonal ring (2.46 Å)) through pristine and defective graphene by investigating the effects of charge and geometry on the energy barrier and kinetic properties in the penetration processes.

II. Computational method

All calculations were performed with the Quantum-Espresso program using periodic boundary conditions. We used a Perdew–Wang 91(PW91) gradient-corrected functional with energy cutoffs for the smooth parts of the wavefunctions and densities of 35 and 350 Ry. In graphite, we sampled the Brillouin zone with a $12 \times 12 \times 10$ k-point mesh while $4 \times 4 \times 1$ sampling in a 5×5 supercell (50 C atoms) was used for graphene. The theoretical equilibrium graphite lattice parameters and the optimized C–C bond length were found to be $a = b = 2.466$ Å, $c = 6.802$ Å and 1.424 Å, respectively, in good agreement with the experimental values[19]

[a] *Soft Matter Research Center and Department of Chemistry, Zhejiang University, Hangzhou 310027, P. R. China. E-mail: liuyingch@zju.edu.cn*
[b] *Department of Physics and Department of Chemistry, University of North Texas, Denton, TX, and CSMD, Oak Ridge National Laboratory, Oak Ridge, TN, USA*

(2.456, 6.696, and 1.418 Å, respectively). The reaction pathways for H diffusion were calculated using the climbing-image nudged elastic band (CI-NEB) method with 7 images for each reaction pathway. We also calculated the partial density of states (PDOS) and charge density difference for the initial, transition, and final states. The kinetic properties were calculated from the phonon frequencies at the Γ point of the Brillouin zone center by a method that combines density functional theory (DFT) and harmonic transition state theory (hTST).[11] We calculated the potential energy profile for the adsorption of a hydrogen atom on a hollow site at various distances from the graphene to test the effect of the supercell size first. The energy barriers were found to be 2.64 and 2.61 eV for the 5×5 and 8×8 supercells, respectively. The small difference of these values indicates that a 5×5 supercell is sufficient to get the required accuracy in the energetics of these systems.

III. Results and discussion

A. Physisorption

1. H. We first considered the tunneling of a hydrogen atom through a graphene sheet. Hydrogen physisorbes onto graphene at a distance of 2.86 Å from the center of a hexagonal carbon ring (hollow site), as shown in the images of the initial and final states in Fig. 1a. Using these configurations of the initial and final states (mirror configurations with respect to the graphitic plane) we ran a CI-NEB simulation to identify the diffusion pathway of the hydrogen atom through the system, shown in Fig. 1a. A rather energetic activation energy barrier of 2.86 eV characterizes the resultant path, as the hydrogen atom tunnels directly through the benzene ring of graphene there is a strong electronic interaction between the two systems but no evidence of bonding.

In this process the benzene ring first expands and then shrinks; the diameters of the hexagonal ring in the initial/final and transition states are 2.85 and 2.91 Å, respectively. At the transition state, the hydrogen atom is in the center of the hexagonal ring at a distance of ~1.46 Å from each of the carbon atoms. The hexagonal ring expands when the hydrogen atom moves closer to the graphene plane, and contracts when the hydrogen moves away from it.

The strong orbital overlap between the electrons from the H atom and the graphene is evident from the analysis of the PDOS for the initial and transition states, shown in Fig. 1b. In the initial state, there is not significant overlap between the hydrogen and graphene states, which means there is a very weak interaction between the two systems. At the transition state, the PDOS of the six nearest carbon atoms completely overlap, so the interaction of the hydrogen atom and each of the six nearest carbon atoms is identical. It can be seen that the PDOS of the C2s and H1s, as well as the C2p and H2s have overlapping peaks at −21.62 and 2.08 eV, showing the strong interaction between the hydrogen atom and graphene sheet at the transition state.

2. H^+. In the case of proton tunneling we clearly expect an easier particle tunneling through the graphene sheet. Similarly to the atomic hydrogen case, a proton adsorbs in the center of a hexagonal carbon ring at a height of about 2.10 Å from the graphene plane. The shorter distance from the plane suggests a stronger bonding interaction between the proton and the graphene electrons. Although the energy barrier for penetration is still high, 2.21 eV, the proton experiences bond formation and breakage with the carbon atoms of graphene rather than direct penetration, as in the case of hydrogen. As before, the diffusion process is accompanied by an initial expansion and then a contraction of the benzene ring upon proton tunneling. This time, however, the diffusion pathway is not through the center of a benzene ring, and the proton–C distance at the transition state ranges between 1.23 and 1.68 Å, so that C atoms in the ring will interact differently with the proton depending on their location. Because of this, the six carbon atoms can be divided into three groups: the first, the second, and the third nearest neighbors, each group containing two atoms. This distinction is useful in analyzing the PDOS, illustrated in Fig. 2a. The PDOS of the carbon atoms in each group show that the closer the distance the larger the intensity of the peak overlapping with the proton at −20.91 and 3.47 eV.

To further confirm the differences between the tunneling processes of a hydrogen atom and a proton, the energy barriers were also calculated from the curves of the potential energy *vs.* distances of the hydrogen/proton from graphene in Fig. 2b, which is a pure physical process without graphene relaxation. By comparing the results with those from the CI-NEB method, it can be seen that the system relaxation in the CI-NEB method has little influence on the energy barrier for H atom tunneling, 2.64 eV *vs.* 2.86 eV, but it has a significant effect on proton

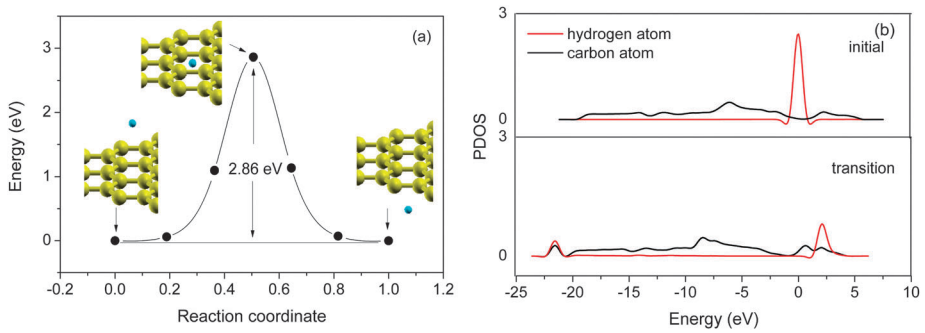

Fig. 1 (a) Reaction energy profile for a hydrogen atom directly penetrating a graphene sheet. (b) PDOS of initial and transition states for hydrogen penetration (zero energy corresponds to the Fermi level).

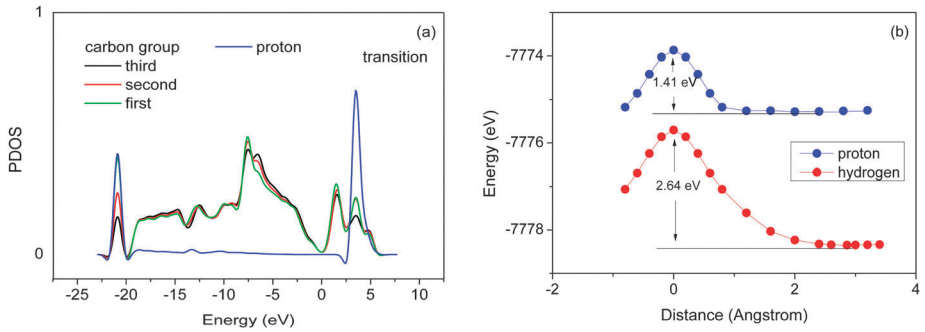

Fig. 2 (a) PDOS of the transition state for proton penetration (zero energy corresponds to the Fermi level). (b) Potential energy *vs.* distances of the hydrogen/proton from the graphene while passing through the center of a hexagonal carbon ring of perfect graphene.

tunneling, 1.41 eV *vs.* 2.21 eV, due to its chemical reactivity. The interaction time between the proton and graphene may be long enough for system relaxation, which may result in a slower motion of the proton and a higher energy barrier in the CI-NEB method than that from the potential energy curve for a purely physical process without graphene relaxation. Therefore, the results from the two approaches are consistent and they indicate that the energy barrier for proton penetration is smaller than for hydrogen penetration, which indicates that a proton penetrates more easily than a hydrogen atom through graphene.

To better understand the natural difference between the systems of hydrogen–graphene and proton–graphene at the electronic level, we have analyzed the charge density differences for the two systems, shown in Fig. 3, where red indicates electron accumulation, and blue electron depletion. The electron density differences are evaluated as = (H or H^+–graphene) − (graphene) − (H or H^+). The charge density differences for the initial and transition states of hydrogen–graphene are shown in Fig. 3a and c, while Fig. 3b and d show the proton–graphene systems. Comparing the initial states of the two systems, as shown in Fig. 3a and b, the hydrogen atom primarily interacts with the carbon atoms of the hexagonal ring below, but this trend is not obvious in the system of proton–graphene, where the interaction is clearly much more delocalized. The electron density differences, as shown in Fig. 3c and d for the transition states of the two systems, are consistent with their geometries and PDOS. The electron density difference is highly symmetrical in Fig. 3c, while it is close to one side of the hexagonal ring and is asymmetric in Fig. 3d. The electron density differences of the hydrogen and proton suggest that the interactions between the hydrogen/proton and the carbons of graphene are different. Therefore, their mechanisms of passing through graphene are different due to the effect of charge.

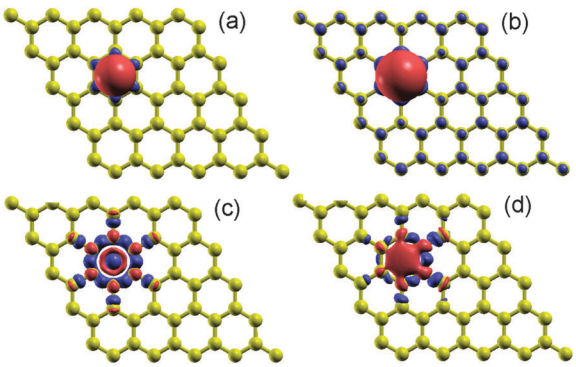

Fig. 3 Electron density differences for the penetration into a graphene sheet by a hydrogen and proton. Initial and transition states for the hydrogen–graphene system are (a) and (c) and of those for the proton–graphene system are (b) and (d). Red indicates electron accumulation, blue indicates electron depletion.

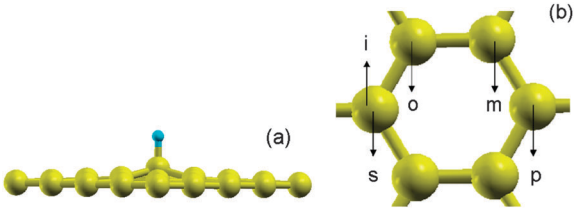

Fig. 4 The model (a) represents the optimized structure for a hydrogen atom chemisorbed on graphene. The different chemisorption sites of a H atom are shown in (b): the sites of s, *o*, *m* and *p* are on the opposite side of the graphene sheet, compared with the site i.

B. Chemisorption

Besides the physisorption case studied above, a hydrogen atom can be easily adsorbed on graphene with a small energy barrier of 0.18 eV[9] forming a stable C–H bond. In agreement with previous calculations,[11] we found the distance of the C–H bond to be approximately 1.13 Å and the carbon atom bonded with the hydrogen relaxed out of the sheet plane by 0.47 Å, which can be seen in Fig. 4a.

For modeling the migration of the hydrogen atom in a chemisorbed state from one side to the other side using CI-NEB calculations, four different final configurations were chosen corresponding to the same initial configuration (i): the same sublattice (s), *ortho* (*o*), *meta* (*m*), and *para* (*p*), shown in Fig. 4b. And the four corresponding paths are shown in Fig. 5. In comparison, the three diffusion routes (i → s, i → *m*, i → *p*) all involve the expansion of the hexagonal ring and a rotation of a C–H bond from one side to the other side of the graphene, so their energy barriers are almost the same (4.54 eV, 4.55 eV, 4.54 eV, respectively). More importantly the penetrations do not occur in the center of the hexagonal ring of graphene. However, in the diffusion route of i → *o*, the graphene plane distorts with

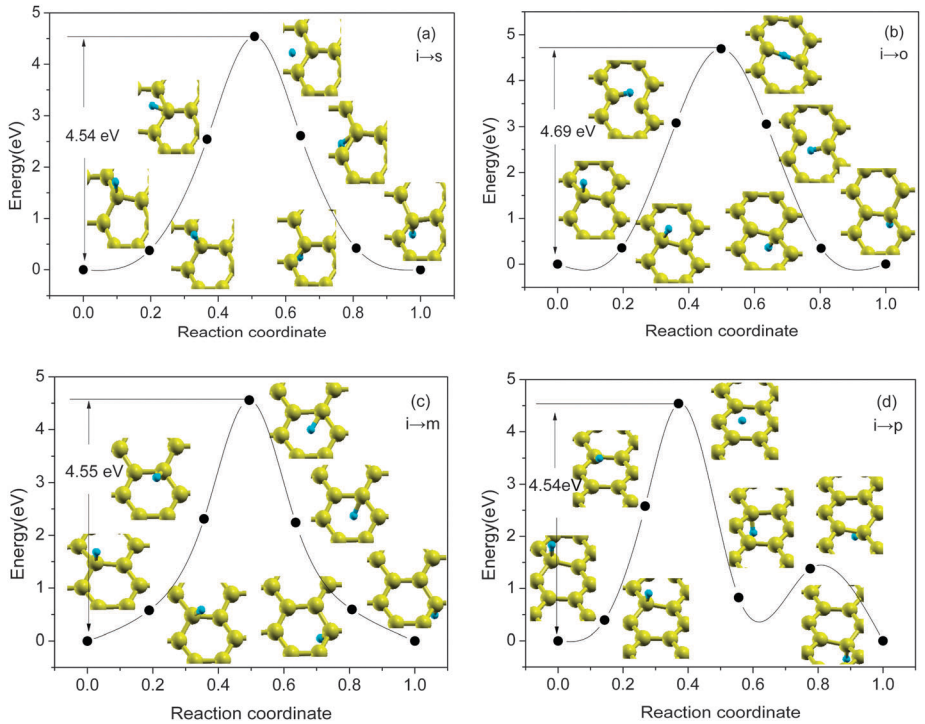

Fig. 5 Four migration pathways and energy barriers for a hydrogen atom from one side to the opposite side of graphene in chemisorption: i → s, i → *o*, i → *m*, and i → *p*.

the formation of two seven-membered rings, which is why the energy barrier (4.69 eV) is a little larger than those for the other routes mentioned above. Clearly, if the H atom chemisorbs on the graphene sheet, more energy is required to overcome the chemical bond breaking in order to tunnel compared to the physical adsorption case, so tunneling is almost forbidden. Similar behavior is observed also in the case of the proton (the route of i → s, as an example), where the migration process is also accompanied by the expansion of the hexagonal ring and a rotation of a C–H bond from one side to the other not exactly through the center of the hexagonal ring, the important difference is that the energy barrier is smaller than that for hydrogen (3.44 eV *vs.* 4.54 eV), indicating that tunneling in this case is still quite unlikely unless the particles are given a sufficiently high energy to allow the tunneling.

C. Effect of graphene defects on the energy barrier and kinetic properties

Structural defects in graphene are common and can be a result of the growth procedure used to produce the samples[20] or they can be created through irradiation by electrons or ions.[21] Of course, we expect that extended geometrical defects will impact the tunneling barriers for both H and H^+. Indeed, the penetration barrier of He through defective graphene has been found to decrease exponentially with the size of the defects,[13] and Li ions can enter nanotubes through topological defects consisting of at least enneagons.[14] We considered two defective configurations: thermodynamically stable divacancies (DV) and 555-777 (one reconstruction from a DV) defects.[22] We found that the hydrogen atom is easily adsorbed on graphene because of the influence of the vacancies; thus, it is more difficult to see the direct passage of hydrogen through the graphene from CI-NEB calculations. That is why the interaction potential was studied to capture the effect of a defect in Fig. 6.

Compared to the energy barrier of 2.64 eV for the passage of a hydrogen atom through the center of a carbon hexagon of perfect graphene, we found that the barrier reduced largely to 0.66 eV for DV and 1.17 eV for 555-777 defects. As shown in Fig. 6a and b, the plot of potential energy as a function of the distance of a hydrogen from graphene indicates that a larger defect size results in a smaller penetration barrier. For the defect sites of defective graphene the hydrogen atom interacts at different distances, there are stable states at about 1.2 Å in Fig. 6a and about 1.5 Å in Fig. 6b. That is to say the potential energy is at its lowest point when the hydrogen atom moves close to the defect sites. At this point, the interaction between hydrogen and the graphene with a defect is strongest. Their electrons would be mutually exclusive if the hydrogen atom moved closer. Moreover, the influence of the defect extends beyond the defect site. In fact, a hydrogen atom penetrates with a reduced barrier through a carbon ring next to a DV (Fig. 6c) or a 555-777 defect (Fig. 6d): 2.08 *vs.* 2.64 eV for the DV and 1.72 *vs.* 2.64 eV for the 555-777 defect. These results are consistent with previous studies[22] that indicated the influence of a defect on the energetics of interacting atoms can be as far as 2–3 nm. Different types of sites were compared, from examining the defect sites (Fig. 6a and b) *vs.* the sites near the defect sites (Fig. 6c and d), it seems that a hydrogen atom is captured by a defect site but is released from a hexagonal ring site close to the defect site. Here defects are considered to be crucial in affecting the behavior of hydrogen penetration.

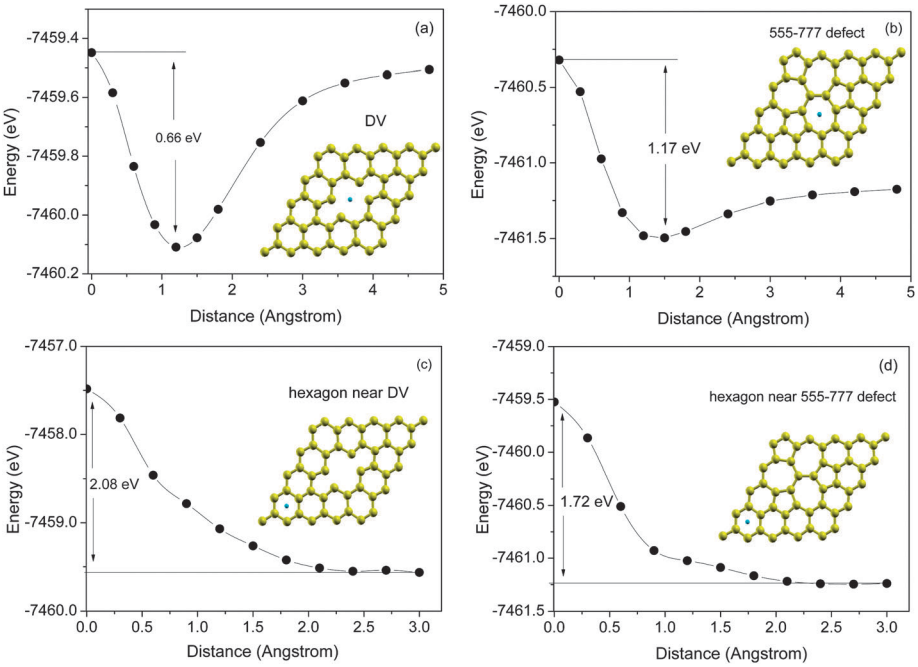

Fig. 6 The potential barrier *vs.* distance of hydrogen from graphene for the penetration of a hydrogen atom through the defective graphene, the insets represent different structures of defective graphene and different sites of the hydrogen atom passing through: DV (a), 555-777 defect (b), a hexagon near DV (c), and a hexagon near a 555-777 defect (d).

Finally, to understand the effect of defects on the kinetic properties of the interacting system, we have addressed the jump frequency for hydrogen penetrating a hexagonal center of perfect graphene and a DV defect using the Arrhenius form:

$$k = A\exp\left(-\frac{E_a}{k_B T}\right) \quad (1)$$

Here A is a pre-exponential factor, E_a is the apparent activation energy

$$E_a = \Delta E_P + \frac{1}{2}\sum_{i=1}^{3N-1} h\omega_i^S - \frac{1}{2}\sum_{i=1}^{3N} h\omega_i^I \quad (2)$$

where ΔE_p is the energy barrier calculated by DFT directly, ω_i is the frequency of the ith vibrational mode and S, I indicate the saddle-point and initial states, respectively, k_B is the Boltzmann constant and T is the temperature. From a quantum mechanical consideration based on modified hTST, the pre-exponential factor can be written as[11]

$$A = \frac{k_B T}{h}\frac{\prod_{i=1}^{3N}\left(1-\exp\left(-\frac{h\omega_i^I}{k_B T}\right)\right)}{\prod_{i=1}^{3N-1}\left(1-\exp\left(-\frac{h\omega_i^S}{k_B T}\right)\right)} \quad (3)$$

Fig. 7 illustrates the jump frequency calculated for a hydrogen atom tunneling through a hexagon in perfect graphene and through a DV defect in the temperature range of 273–1000 K. There is a linear relationship between the logarithm of jump frequency and the inverse temperature. The relationship of k(DV) > k(perfect) holds through all the temperatures and at room temperature (298 K), the penetration frequencies are 218 Hz and 1.2×10^{-34} Hz, respectively. This reveals that a hydrogen atom will be moving through a DV defect at more than 200 hops per second at room temperature, but it is almost not able to pass through the center of a hexagon of prefect graphene. These results are consistent with their penetration energy barriers, in that the higher energy barrier is, the smaller the possibility of penetration becomes. Further, there are many different types of vacancies, the shape and size of which will have a specific impact to a certain extent. Therefore, we consider that defects in graphene that allow hydrogen penetration could be used in separation applications.

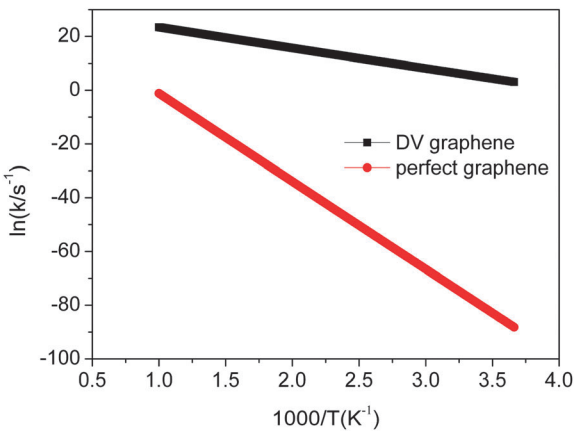

Fig. 7 The logarithm of the jump frequency of a hydrogen passing through a hexagonal center of perfect graphene (red line) and a DV graphene defect (black line) as a function of the inverse of temperature.

IV. Conclusion

In summary, hydrogen/proton tunneling through a graphene sheet was studied to explore the permeability of a single graphene sheet. The effects of charge, adsorption states, and defects on the tunneling energy barriers were discussed. The hexagonal ring of graphene expands when a hydrogen atom passes through it, but a proton penetrates more easily than a hydrogen into graphene. It is more difficult for a hydrogen atom to tunnel through the graphene sheet once a C–H bond is formed. Defects can greatly reduce the penetration energy barrier and the actual region of influence of the defect extends beyond the defect site, for example hydrogen at room temperature will be moving through DV graphene at more than 200 hops per second. This result provides a new purpose for graphene in potentially revolutionary applications.

Acknowledgements

This work was financially supported by the National Natural Science Foundation of China (Nos. 20876132, 20976150).

References

1 A. K. Geim, *Science*, 2009, **324**, 1530.
2 J. O. Sofo, A. S. Chaudhari and G. D. Barber, *Phys. Rev. B: Condens. Matter Mater. Phys.*, 2007, **75**, 153401.
3 F. Schwierz, *Nat. Nanotechnol.*, 2010, **5**, 487.
4 A. K. Singh and B. I. Yakobson, *Nano Lett.*, 2009, **9**, 1540.
5 Z. Waqar, *J. Mater. Sci.*, 2007, **42**, 1169.
6 A. Ito, Y. Wanga, S. Irle, K. Morokuma and H. Nakamura, *J. Nucl. Mater.*, 2009, **390–391**, 183.
7 H. Nakamura, A. Takayama and A. Ito, *Contrib. Plasma Phys.*, 2008, **48**, 265.
8 C. P. Herrero and R. Ramírez, *Phys. Rev. B: Condens. Matter Mater. Phys.*, 2009, **79**, 115429.
9 Y. Miura, H. Kasai, W. A. Diño, H. Nakanishi and T. Sugimoto, *J. Phys. Soc. Jpn.*, 2003, **72**, 995.
10 L. Chen, A. C. Cooper, G. P. Pez and H. S. Cheng, *J. Phys. Chem. C*, 2007, **111**, 18995.
11 L. F. Huang, M. Y. Ni, X. H. Zheng, W. H. Zhou, Y. G. Li and Z. Zeng, *J. Phys. Chem. C*, 2010, **114**, 22636.
12 J. Scott Bunch, S. S. Verbridge, J. S. Alden, A. M. van der Zande, J. M. Parpia, H. G. Craighead and P. L. McEuen, *Nano Lett.*, 2008, **8**, 2458.
13 O. Leenaerts, B. Partoens and F. M. Peeters, *Appl. Phys. Lett.*, 2008, **93**, 193107.
14 V. Meunier, J. Kephart, C. Roland and J. Bernholc, *Phys. Rev. Lett.*, 2002, **88**, 075506.
15 D. Jiang, V. R. Cooper and S. Dai, *Nano Lett.*, 2009, **9**, 4019.
16 J. Schrier, *J. Phys. Chem. Lett.*, 2010, **1**, 2284.
17 S. P. Koenig, L. Wang, J. Pellegrino and J. Scott Bunch, *Nat. Nanotechnol.*, 2012, **7**, 728.
18 A. W. Hauser and P. Schwerdtfeger, *J. Phys. Chem. Lett.*, 2012, **3**, 209.
19 R. W. G. Wyckoff, *Crystal structures*, Interscience Publishers, New York, 1963.
20 F. Banhart, J. Kotakoski and A. V. Krasheninnikov, *ACS Nano*, 2011, **5**, 26.
21 J. R. Hahn and H. Kang, *Phys. Rev. B: Condens. Matter Mater. Phys.*, 1999, **60**, 6007.
22 O. Cretu, A. V. Krasheninnikov, J. A. Rodríguez-Manzo, L. T. Sun, R. M. Nieminen and F. Banhart, *Phys. Rev. Lett.*, 2010, **105**, 196102.